International Journal of Engineering Science 61 (2012) 156–170

Contents lists available at SciVerse ScienceDirect

International Journal of Engineering Science

journal homepage: www.elsevier.com/locate/ijengsci

A diffusion and curvature dependent surface elastic model with application to stress analysis of anode in lithium ion battery

Jin-Liang Zang, Ya-Pu Zhao *

State Key Laboratory of Nonlinear Mechanics, Institute of Mechanics, Chinese Academy of Sciences, Beijing 100190, China

ARTICLE INFO

Article history:
Received 29 February 2012
Accepted 2 April 2012
Available online 23 July 2012

Keywords:
Surface elastic model
Tolman length
Lithium ion battery
Nanostructured Si electrode
Pulverization

ABSTRACT

The present paper investigates the influences of surface tension and the stress distribution in the bulk induced by the surface tension, surface curvature and ions' diffusion on the elastic properties of nanostructures. In the electro-chemical diffusion process, the surface tension, ions diffusion and stress distribution will strongly dependent with each other. Here, considering the curvature effect, a surface elastic model coupled with the ions diffusion is proposed. In the model, the coupling between the stress and ions diffusion is revealed through the chemical potential variation. To reveal the curvature effect on the surface energy, a Tolman length for solid is introduced. As a typical application of the model, we analyze the stress distributions in the silicon anode of the lithium ion battery. In recent years, silicon, due to large theoretical energy density, becomes one of the promising candidate anode materials. However, huge volume changes of silicon in charging and discharging process hinders its application. We depict the stresses provenance and evolution of hollow nanosphere and nanotube induced by lithium ions diffusion. Self-buckling induced by surface stresses of the two nanostructures is also taken into consideration. Critical buckling sizes are analyzed. All results show that hollow nanosphere will be a more suitable structure for electrode. Finally, a new dimensionless number κ related to Young's modulus, Tolman length and surface energy is proposed to estimate the relative importance of the Tolman length with the intrinsic material length. It is believed that the diffusion and curvature dependent surface elastic model will be a powerful tool to investigate the diffusion behaviors in nanostructured electrode.

1. Introduction

Rechargeable lithium ion batteries become the most suitable energy carrier for portable electro-equipments, electromobiles and high performance computing, not only for the high energy density and low cost, but also for the environmental needs for energy storage (Nazri & Pistoia, 2003). However, the low energy density of traditional carbonaceous materials (for graphite 372 $mAhg^{-1}$) as the anode material for commercial lithium ion batteries cannot meet the requirements for more applications and has become the choke point for developments of batteries. Lots of high capacity substitutes to carbonaceous materials were investigated (Bruce, Scrosati, & Tarascon, 2008), such as antimony (660 $mAhg^{-1}$) (He et al., 2007), tin (994 $mAhg^{-1}$) (Kwon, Kim, Kim, Lee, & Cho, 2006). Compared with these materials, energy density of silicon is one order of magnitude higher, which is about 4200 $mAhg^{-1}$ (Boukamp, Lesh, & Huggins, 1981). Therefore, silicon will be a more suitable promising anode material. Nevertheless, loss of electrical contact due to the fracture and crack induced by huge volume

* Corresponding author.
E-mail address: yzhao@imech.ac.cn (Y.-P. Zhao).

0020-7225/$ - see front matter © 2012 Elsevier Ltd. All rights reserved.
http://dx.doi.org/10.1016/j.ijengsci.2012.06.018

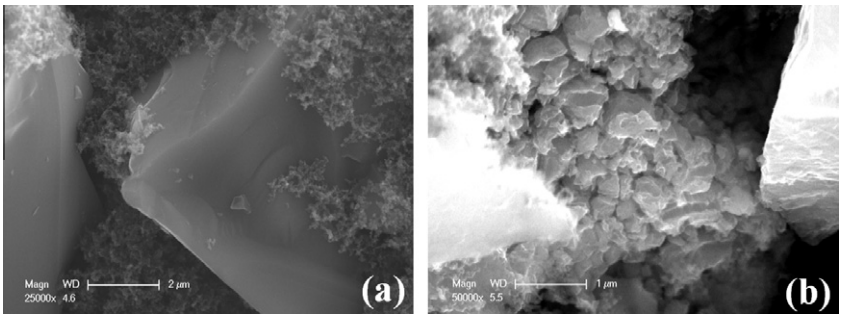

Fig. 1. Stress-induced pulverization of 1–5 μm Silicon particles cycled at ~0.05 C for (a) 0 cycle and (b) 200 cycles.

change (~400%) in charging and discharging cycles hinders its application. During the charging and discharging process, the Li ions move from one electrode through electrolyte to the other. The electrons to-and-fro movements induce the current flow in circuit. The silicon electrode deforms hugely because large number of Li ions jam into the lattice and form full charged state of $Li_{22}Si_5$. The Young's modulus of silicon decreases in an approximately linear manner with increasing Li concentration leading to significant elastic softening (Shenoy, Johari, & Qi, 2010). The lattices of electrodes are always constrained by the substrate, or the mismatch between grains of different crystalline orientations (Hu, Zhao, & Suo, 2010). The stress field is induced when the Li ions keep diffusing in and out of the electrodes. Cracks and fragmentation gradually form. Several cycles latter, the electrode will break into pieces even into powders. Battery failure occurs due to loss of electrical contact. Fig. 1 is a scanning electron microscope picture taken in our experiments for silicon particles with average particle sizes 1–5 μm cycled at ~0.05 C for 0 cycle and 200 cycles, which vividly show the pulverization process.

In recent years, researches demonstrated that using nanostructured electrode can effectively circumvent the fragmentation. In the low-dimensional nanostructures, like nanoparticles, nanowires and nanofilms, the surface-to-volume ratios are very large. The surface effects will significantly affect the properties of the nanomaterials. Morozov and his coworkers established the linear and nonlinear theory of shells with the surface stresses and proved that the surface stresses are responsible for the size effect, especially in modeling nanostructures (Altenbach & Eremeyev, 2011; Altenbach, Eremeyev, & Morozov, 2009; Altenbach, Eremeyev, & Morozov, 2010). Some previous researches have proved that nanostructures can accommodate the volume changes well and have longer stability in terms of cycle life and less fading of capacity (Chan et al., 2008; Kasavajjula, Wang, & Appleby, 2007; Song et al., 2010; Teki et al., 2009). Consequently, it is necessary to clarify the provenances and evolutions of stresses induced by ions diffusion in nanoscale electrode and, further, explore more suitable nanostructures. At the very beginning, many researchers paid more attentions on the diffusion in the solid structures. Li and Mehl studied the diffusion induced stresses in several solid microstructures (Li & Mehl, 1978). Paukshto established a coupled nonlinear theory of diffusion in elastic media and provided some analytical solutions (Paukshto, 1999). Chu and Lee investigated effect of chemical stresses on diffusion and showed that chemical stresses enhance the mass transfer due to increasing diffusivity (Chu & Lee, 1994). Yang studied the interactions between the diffusion and chemical stresses and established a relationship between hydrostatic stress and concentration of solute atoms (Yang, 2012). Furthermore, he used the linear elasticity theory investigating the breakage behaviors in the active materials in the battery (Yang, 2010). Recently, Haftbaradaran et al. got the relation of electrode size and charging rate, and proved that a surface locking instability once the product between electrode dimension and charging rate exceeds a critical value (Haftbaradaran, Gao, & Curtin, 2010). However, with decreasing size of structure to nanoscale, surface effect plays a significant role that has effect on behaviors of structures. Cheng et al. found that the effects of surface tension on diffusion induced stresses have much effect on the stresses distribution if the structure in nanometer ranges (Cheng & Verbrugge, 2008; Cheng & Verbrugge, 2009). They also examined the crack formation in different scale electrodes (Li, Dozier, Li, Yang, & Cheng, 2011).

However, all researches mentioned have paid no attention on surface energy variation in nanoscale caused by diffusion and curvature. Tolman found that for a nanosize liquid droplet, the surface energy will be affected by the curvature obviously (Tolman, 1949). With decreasing of droplet size, the curvature modification cannot be neglected. Compared to nanodroplet, the energy in nanoscale solid structures is also sensitive with the bond length or bond angle between atoms. The surface energy of a curved surface will be quite different from its planer value and the similar modification also should be introduced into a solid structure. Moreover, diffusion of ions on the surface will cause surface chemical potential and the surface strain energy variation. Considering the electrochemistry reaction in the battery, electromotive force of the battery can be calculated through the chemical potential difference of two electrodes which can be represented by $\Delta G = -E_e F$. ΔG is the Gibbs free energy, E_e is the electromotive force of the battery and F is Faraday constant. During the charging and discharging process, accompanying by the ions moving into and out the electrode, the free energy of the electrode will change. Therefore, considering structure curvature and ions diffusion in nanostructure, a suitable surface elastic model is still not available and a better understanding is needed.

In the present paper, based on the previous work (Wang & Zhao, 2011; Wang, Zhao, & Huang, 2010), a surface elastic model coupled with diffusion, curvature effect and residual stress is firstly proposed. Two typical nanostructures: hollow

nanosphere (HNS) and nanotube (NT) were analyzed using this model. The origination and evolution of stresses in HNS and NT induced by Li ions diffusion were depicted. Furthermore, critical buckling sizes of the two structures under the residual stresses were analyzed. Using HNS, compared with the NT, will significantly reduce the magnitude of effective von Mises stress under the same concentration of Li ions. Meanwhile, if the wall-thickness of HNS and NT is same, the critical buckling radius of HNS will be larger than NT. A variety of choices in radius allow the HNS have more flexibility in designing and manufacturing, Thus, HNS becomes a more suitable structure for electrode from the mechanical view.

2. Diffusion and curvature coupled surface elastic model

In this work, we use Gibbs surface model (Gibbs, 1961) which is modeled as a two-dimensional (2D) geometrical boundary of bulk which extends uniformly right up to the mathematical surface with no thickness. The physical properties of the geometrical surface are assigned to preserve the total physical properties of the system. The geometry and kinematics of a deformable surface is similar with what have been proposed in previous work (Wang & Zhao, 2011; Wang et al., 2010). Detailed expressions of these notations are explained in Appendix A. In this paper, three surface stress tensors were introduced, namely surface Cauchy stress tensor $\boldsymbol{\sigma}_s$, the first surface Piola–Kirchhoff stress tensor $\mathbf{S}_s$ and the second surface Piola–Kirchhoff stress tensor $\mathbf{T}_s$, in which $\boldsymbol{\sigma}_s$ is the force measured per unit length in current configuration, $\mathbf{S}_s$ and $\mathbf{T}_s$ are in reference configuration. $\mathbf{C}_s = \mathbf{F}_s^T \cdot \mathbf{F}_s$ is surface deformation tensor in which $\mathbf{F}_s$ is surface deformation gradient tensor. $\mathbf{E}_s$ is surface strain tensor in reference configuration. These three stress tensors satisfy the following work conjugate relations:

$$\dot{w}_s = J_2 \boldsymbol{\sigma}_s : \dot{\mathbf{E}}_s = \mathbf{S}_s : \dot{\mathbf{F}}_s = \frac{1}{2}\mathbf{T}_s : \dot{\mathbf{C}}_s, \tag{1}$$

where γ is the surface energy density in current configuration, J_2 is the ratio between the area elements of after and before deformations which is the second invariant of tensor $\mathbf{U}_s$ (see Appendix) and $w_s = J_2\gamma$ is the surface energy per unit area of surface A_0 in reference configuration. The three surface stresses satisfy the following relations

$$\mathbf{S}_s = \mathbf{F}_s \cdot \mathbf{T}_s, \boldsymbol{\sigma}_s = \frac{1}{J_2}\mathbf{F}_s \cdot \mathbf{T}_s \cdot \mathbf{F}_s^T. \tag{2}$$

For the surface, we can use the work conjugate relations to deduce constitutive relations. Generally, the surface energy density γ is a function of the $\mathbf{U}_s$, furthermore, γ can be written as a function of J_1, J_2 for an isotropic surface, in which J_1 is the first invariant of $\mathbf{U}_s$ ($J_1 = \mathrm{tr}\mathbf{U}_s$). Under the Lagrangian description, the constitutive relation can be written as

$$\mathbf{T}_s = 2\frac{\partial(J_2\gamma)}{\partial \mathbf{C}_s}. \tag{3}$$

For small deformations, the J_1, J_2 can be rewritten as a function of $\mathbf{E}_s$:

$$J_1 = 2 + \mathrm{tr}\mathbf{E}_s, \quad J_2 = 1 + \mathrm{tr}\mathbf{E}_s + \det \mathbf{E}_s. \tag{4}$$

γ also can be expanded as a function of J_1, J_2 and the surface concentration of Li ions C_s:

$$\gamma = \gamma_0 + \gamma_1(J_1 - 2) + \gamma_2(J_2 - 1) + \frac{1}{2}\gamma_{11}(J_1 - 2)^2 + \gamma_{12}(J_1 - 2)(J_2 - 1) + \frac{1}{2}\gamma_{22}(J_2 - 1)^2 + F(C_s) + \cdots, \tag{5}$$

where $F(C_s)$ is the surface energy variation caused by ions diffusion (Belova & Murch, 1995):

$$F(C_s) = \gamma_3 C_s + \gamma_{31} C_s(J_1 - 2) + \gamma_{32} C_s(J_2 - 1) + \gamma_{33} C_s^2. \tag{6}$$

Therefore, from the Eqs. (3)–(6) and neglecting higher-order small quantities, the surface constitutive relation can be expressed as

$$\mathbf{T}_s = 2\frac{\partial(J_2\gamma)}{\partial \mathbf{C}_s} = \gamma_0^* \mathbf{I}_0 + (\gamma_0^* + \gamma_1^*)\mathrm{tr}(\mathbf{E}_s)\mathbf{I}_0 + (\gamma_1 - 2\gamma_0^*)\mathbf{E}_s + \alpha C_s \mathbf{I}_0, \tag{7}$$

where $\gamma_0^* = \gamma_0 + \gamma_1 + \gamma_2$, $\gamma_1^* = \gamma_1 + 2\gamma_2 + \gamma_{11} + 2\gamma_{12} + \gamma_{22}$, $\alpha = \gamma_3 + \gamma_{31} + \gamma_{32}$. The surface energy in the absence of the external loading γ_0, residual surface stress γ_0^* and surface elastic constants γ_1, γ_1^* are material properties intrinsic to the solid (Miller & Shenoy, 2000) α is a constant which can reveal the diffusion properties of an isotropic surface.

What is more, as mentioned, the surface energy γ should be modified for a curved surface, especially in nanosize. Tolman put forward an equation to calculate surface energy for a curved surface of a droplet (Tolman, 1949). In Tolman's work, based on the Kelvin relation to describe the relation between pressure difference and curvature, the expression for the dependence of surface tension on radius can be written as Gibbs–Tolman–Koenig–Buff (GTKB) differential equation (Mandell & Reiss, 1975):

$$\frac{1}{\gamma_0}\frac{d\gamma_0}{dr} = \frac{\frac{2\delta}{r^2}\left(1 + \frac{\delta}{r} + \frac{\delta^2}{3r^2}\right)}{1 + \frac{2\delta}{r}\left(1 + \frac{\delta}{r} + \frac{\delta^2}{3r^2}\right)}, \tag{8}$$

where r is the curvature radius for a surface, and δ is the Tolman length which denotes the extent by which the surface tension of a small liquid drop deviates from its planar value. Integrating Eq. (8) from $r = \infty$ corresponding to a planar surface to any radius r, and assuming γ^{∞} is the surface energy for a planar surface, the integral form for the Eq. (8) can be rewritten as

$$\ln\frac{\gamma_0}{\gamma^{\infty}} = \int_{\infty}^{r} \frac{\frac{2\delta}{r^2}\left(1+\frac{\delta}{r}+\frac{\delta^2}{3r^2}\right)}{1+\frac{2\delta}{r}\left(1+\frac{\delta}{r}+\frac{\delta^2}{3r^2}\right)}dr. \tag{9}$$

Considering δ is a quantity of the order of average distance between atoms and treating it as a constant, neglecting δ^2 and δ^3 in the integration, we can get a simple equation:

$$\gamma_0 = \frac{\gamma^{\infty}}{1+\frac{2\delta}{r}}. \tag{10}$$

Finally, the γ_0 in Eq. (10) will be used in stress calculation. Here, we would like to give some more remarks on Tolman length. In physical view, the δ, which is the difference between the radii of the equimolar surface and the surface of tension, represents the size effect of surface tension. If a solid particle is large enough, the term δ/r in denominator of Eq. (10) is a small quantity and could be neglected. The surface tension will have no deviation from its planar value. However, in nanoscale, the δ/r is not a small quantity, and the surface tension γ_0 will have a huge variation compared with the planar value.

The Tolman length δ is defined as:

$$\delta = R_e - R_s, \tag{11}$$

where R_e and R_s are the radii of the equimolar surface and the surface of tension, respectively. The two radii R_e and R_s can be calculated using molecular dynamics (MD) simulations. The details to calculate the Tolman δ will be given in next part.

The surface concentration of Li ions can be obtained through Fick's second law (Li & Mehl, 1978; Paukshto, 1999)

$$\begin{cases} \bar{\nabla}_s(M_s C_s \bar{\nabla}_s \mu_s) = \frac{\partial C_s}{\partial t}, \\ \mu_s = \mu_{s0} + RT\ln C_s - \frac{1}{2}\mathrm{tr}(\mathbf{T}_s)\bar{S}, \end{cases} \tag{12}$$

where $\bar{\nabla}_S$ is the surface gradient operator in the current configuration, M_s is the molar mobility of solute in the surface, μ_s is the surface chemical potential, μ_{s0} is a constant, R is the gas constant, T is the absolute temperature and $\bar{S}$ is the partial molar area. The chemical potential can be regarded as the reason for the variation of free energy $\Delta G = -E_e F$ in the electrochemical reaction.

The above all are constitutive relations for the surface. Considering a bulk material with the surface properties aforementioned, the surface tension induces a stress field in the bulk. According to Young-Laplace equations, the surface tension will result in a non-classical boundary condition. The boundary condition together with the equations of classical elasticity forms a coupled system of field equations to determine the stress distribution (Gurtin & Murdoch, 1978).

In the reference configuration, the elastic stress field $\mathbf{T}_R$ in the bulk satisfies the generalized Young–Laplace equations which also should be modified due the curvature effect:

$$\mathbf{T}_R \cdot \bar{\nabla}_B = 0 \text{ (in the bulk)}, \tag{13}$$

$$\begin{cases} \mathbf{N}\cdot[\![\mathbf{T}_R]\!]\cdot\mathbf{N} = -\frac{\gamma^{\infty *}}{1+\frac{2\delta}{r}}\mathbf{I}_0 : \mathbf{b}_0 \\ \mathbf{P}_0\cdot[\![\mathbf{T}_R]\!]\cdot\mathbf{N} = -\nabla_{0s}\left(\frac{\gamma^{\infty *}}{1+\frac{2\delta}{r}}\right) \end{cases} \text{(on the surface)}, \tag{14}$$

in which $\bar{\nabla}_B$ is the three-dimensional Laplace operator, $\gamma^{\infty *}$ is residual surface stress for a plane surface, $\mathbf{b}_0$ is the surface curvature tensors and $\mathbf{P}_0 = \mathbf{1} - \mathbf{N}\otimes\mathbf{N}$ s the perpendicular projection of all vectors upon the space of tangential vectors in the reference configuration, $\mathbf{1}$ is the identity tensor in 3D Euclidean space. ∇_{0s} is the surface gradient operator in the reference configuration.

Consequently, to determine the linear elastic constitutive relations for the nanostructure, the constitutive relations should consider the residual stress effect rather than using the classical Hooke's law (Hoger, 1986). For the bulk, the linear elastic constitutive relations can be written as

$$\mathbf{T} = \mathbf{T}_R + L(\mathbf{T}_R, C_B^0) : \mathbf{E} + \alpha_B C_B \mathbf{1}, \tag{15}$$

where $L(\mathbf{T}_R, C_B^0)$ is the incremental elastic modulus for the bulk, $\mathbf{E}$ is the infinitesimal strain, and α_B is a constant which represents the diffusion properties for the bulk. The concentration of Li ions for the bulk can be determined through

$$\begin{cases} \bar{\nabla}_B(M_B C_B \bar{\nabla}_B \mu_B) = \frac{\partial C_B}{\partial t}, \\ \mu_B = \mu_{B0} + RT\ln C_B - \frac{1}{3}\mathrm{tr}(\mathbf{T})\overline{V}, \end{cases} \tag{16}$$

where M_B is the molar mobility for a solute in the bulk, μ_B is the Li ions chemical potential in the body and μ_{B0} is a constant, C_B is the concentration of Li ions in the bulk, $\overline{V}$ is the partial molar volume. In these symbols, the subscript B represents the properties or operators in the bulk.

We can use all relations mentioned above to analyze stress distributions in two nanostructures: HNS and NT for nanostructured electrode of Li ions batteries.

3. Two nanostructured electrodes analyses

Nanostructured electrodes will have genuine potential to make a significant impact on the performance of Li ions batteries. Using nanostructred electrodes can increase the rate of lithium insertion and removal due to the short transportation distance; the high surface-to-volume ratio permits a large contact area with the electrolyte and improves the Li ions' flux across the interface. The huge strain induced by the Li ions' insertion will also be accommodated (Bruce et al., 2008). In previous works, a lot of nanostructured electrodes had been experimentally investigated, for examples, nanofilm, nanowire or nanorod and nanoparticle(Chan et al., 2008; Kasavajjula et al., 2007; Song et al., 2010; Teki et al., 2009). However, in these works, there are little theoretical interpretations and few comparisons for different structures. Moreover, as elucidated, the nanostructures will have extraordinary behaviors due to the surface effect. Therefore, to predict or understand the behaviors of nanostructures, especially in nanostructured electrodes, the theoretical model with surface effect coupled the diffusion should be considered. In this part, we will use the proposed theoretical model to investigate the stress distributions in two structures: HNS and NT, and a comparative study on stress distributions is performed. The structure of this part is organized as follows: for each nanostructure (HNS, NT), we will analyze the stress distributions with different sizes; the Tolman length adopted in analysis is calculated by MD simulations. Afterwards, without considering the MD data of Tolman length, the different Tolman length is assumed and the Tolman effect on stress distributions is depicted. At last, surface stress induced structure self-buckling is discussed for nanostructured electrode stability.

3.1. HNS stress distributions analysis

First, an isotropic HNS with outer radius r_o and inner radius r_i is considered, as illustrated in Fig. 2. The HNS is located in spherical coordinate system (r, θ, φ). The HNS will experience self-stressing due to the surface energy and keep in a residual stress state. Meanwhile, due to the spherical symmetry, surface energy has no effect on the magnitude and distribution of shear stresses for any size. The concentration of Li ions was assumed continuously distributed on the surface and in the bulk. Additionally, the atomic diffusion in solids is much slower than elastic deformation. Therefore, the mechanical equilibrium can be treated as a quasi-static process.

A steady diffusion process was considered, in which the concentration on the inner and outer surfaces were constants C_i, C_o, respectively. Solve the diffusion Eqs 12,16 with initial and boundary conditions:

$$\frac{\partial C_s}{\partial t} = 0, \frac{\partial C_B}{\partial t} = 0, C_s|_{r=r_i} = C_i, C_s|_{r=r_o} = C_o. \tag{17}$$

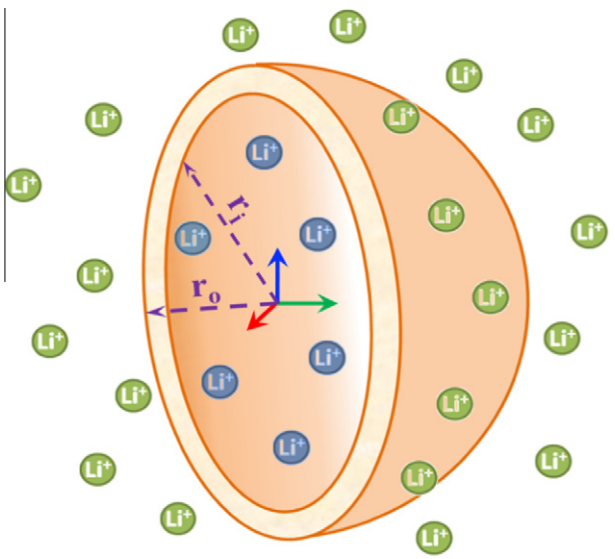

Fig. 2. HNS for the nanostructured electrode.

Then, the Cauchy stresses of HNS in spherical coordinate system (r, θ, φ) are:

$$\begin{cases} \sigma_{rr} = -\frac{E\Omega(C_o-C_i)}{3(1-\nu)}\frac{r_o r_i(r-r_o)(r-r_i)[r_o r_i + r(r_o+r_i)]}{r^3(r_o^3-r_i^3)} + \frac{2\gamma^\infty}{r_i+2\delta}\frac{\frac{r_o^3}{r^3}-1}{\frac{r_o^3}{r_i^3}-1} - \frac{2\gamma^\infty}{r_o+2\delta}\frac{1-\frac{r_i^3}{r^3}}{1-\frac{r_i^3}{r_o^3}} \\ \sigma_{\theta\theta} = \sigma_{\varphi\varphi} = \frac{E\Omega(C_o-C_i)}{3(1-\nu)}\frac{r_o r_i[r_o^2 r_i^2 - 2r^3(r_o+r_i)+r^2(r_o^2+r_o r_i+r_i^2)]}{2r^3(r_o^3-r_i^3)} - \frac{2\gamma^\infty}{r_i+2\delta}\frac{\frac{r_o^3}{2r^3}+1}{\frac{r_o^3}{r_i^3}-1} - \frac{2\gamma^\infty}{r_o+2\delta}\frac{1+\frac{r_i^3}{2r^3}}{1-\frac{r_i^3}{r_o^3}} \end{cases} \tag{18}$$

In the equations, E is the Young's modulus for the isotropic material, ν is the Poisson's ratio and Ω is the partial molar volume of the solute. $A \equiv E\Omega(C_o - C_i)/[3(1-\nu)]$ is a stress induced by the maximum and minimum concentration in the structures. Dividing the characteristic stress A on both sides of the Eq. (18) and using the dimensionless parameters $\delta^* = \delta/r_o$, $\alpha = r/r_o$, $\alpha_i = r_i/r_o$ to obtain the dimensionless stresses:

$$\begin{cases} \sigma^*_{rr} = -\frac{\alpha_i(\alpha-1)(\alpha-\alpha_i)[\alpha_i+\alpha(1+\alpha_i)]}{\alpha^3(1-\alpha_i^3)} + \frac{2\gamma^\infty}{r_o A}\frac{1}{\alpha_i+2\delta^*}\frac{\alpha^{-3}-1}{\alpha_i^{-3}-1} - \frac{2\gamma^\infty}{r_o A}\frac{1}{1+2\delta^*}\frac{1-\alpha_i^3\alpha^{-3}}{1-\alpha_i^3} \\ \sigma^*_{\theta\theta} = \sigma^*_{\varphi\varphi} = \frac{\alpha_i[\alpha_i^2-2\alpha^3(1+\alpha_i)+\alpha^2(1+\alpha_i+\alpha_i^2)]}{2\alpha^3(1-\alpha_i^3)} - \frac{2\gamma^\infty}{r_o A}\frac{1}{\alpha_i+2\delta^*}\frac{0.5\alpha^{-3}+1}{\alpha_i^{-3}-1} - \frac{2\gamma^\infty}{r_o A}\frac{1}{1+2\delta^*}\frac{1+0.5\alpha_i^3\alpha^{-3}}{1-\alpha_i^3} \end{cases} \tag{19}$$

For illustration, the parameters $E = 130$ GPa, $\nu = 0.28$, $\gamma^\infty = 1.4\ \mathrm{Jm}^{-2}$ (Hara, Izumi, Kumagai, & Sakai, 2005) were chosen for silicon. The HNS, whose inner radius is $r_i = 5$ nm and outer radius is $r_o = 10$ nm, is under the diffusion condition $\Omega C_i = 0$, $\Omega C_o = 0.08$.

The Tolman length for the silicon sphere was obtained through MD simulations. The δ was calculated through the definition according to Eq. (11). Like Thompson, Gubbins, Walton, Chantry, & Rowlinson, 1984, the radii of equimolar surface R_e and surface of tension R_s in sphere, respectively, are:

$$\begin{cases} R_e = -\sqrt[3]{\frac{\int_0^\infty r^3\frac{d\rho(r)}{dr}dr}{\rho_B-\rho_g}}, \\ R_s = -\sqrt[3]{\frac{\int_0^\infty r^3\frac{dp(r)}{dr}dr}{p_B-p_g}}, \end{cases} \tag{20}$$

in which $\rho(r)$, $p(r)$ are density and pressure distributions with respect to the radius r. The subscript g represents the properties in the gas phase, which is usually zero at infinity. Within the Eqs. (20), we can see the statistical meaning of R_e and R_s. R_e is defined so that the system contains an equal number of molecules where the density to remain constant at its two respective limiting values on either side of the surface, with a discontinuous change at the surface itself (Thompson et al., 1984). The R_s has the similar meaning as R_e but the difference is that R_s reflects the pressure variation. In simulation, considering the computation cost and small fluctuation of Tolman length in nanoscale, a 5 nm silicon sphere was parameterized within the Tersoff force field (Tersoff, 1988) and all MD runs were carried out by using the large-scale atomic molecular massively parallel simulator (LAMMPS) (Plimpton, 1995). The system was relaxed to a minimum energy configuration, and then thermally equilibrated to 300 K for 100 ps using the Nose-Hoover thermostat (Nose, 1984) with a time step of 1 fs. The distributions of $\rho(r)$, $p(r)$ and the quantities ρ_B, ρ_g, p_B, p_g were obtained with respect to the time average of all simulation progress. In Fig. 3, the square dots are simulated quantities and the solid lines are fitted functions.

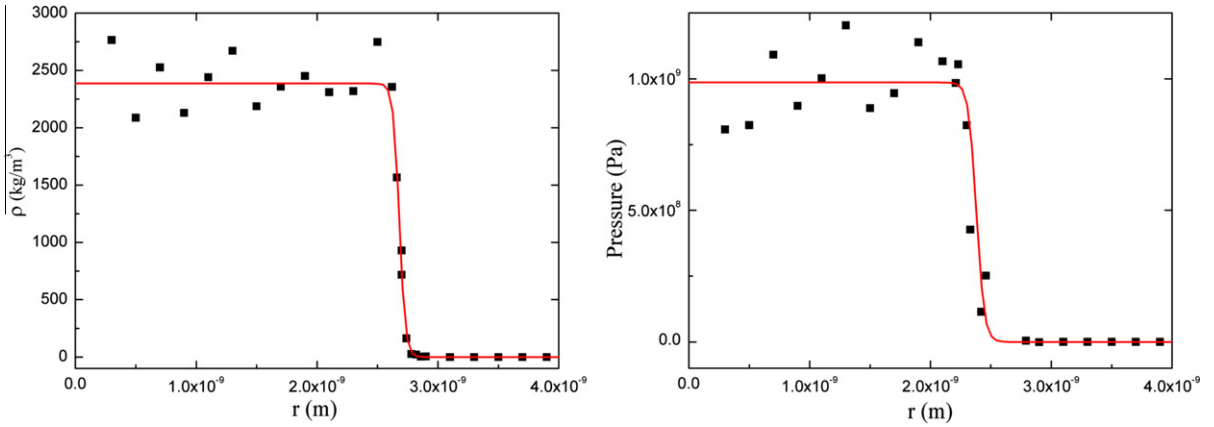

Fig. 3. Density and pressure profiles for the silicon sphere.

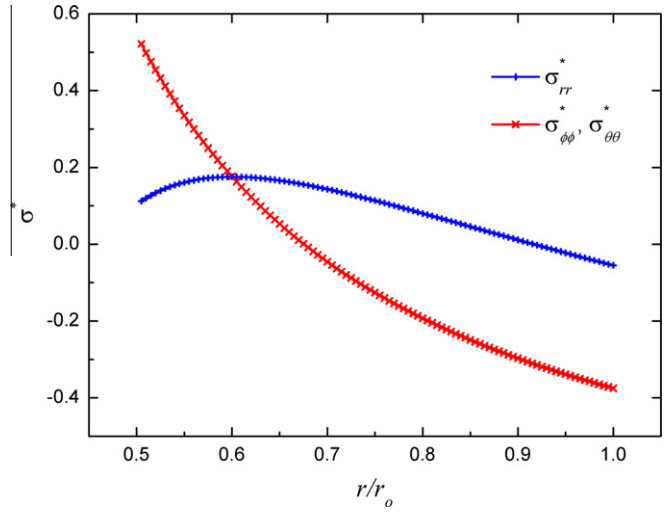

Fig. 4. Stresses distribution in the HNS.

Using the Eqs. 11,20 and the quantities from the simulations, the Tolman length for the nanosphere is obtained, which is δ = 0.293 nm. The lattice constant of diamond structure silicon is 0.543 nm which is one the same order of δ. Finally, we can draw the stress distributions of HNS in Fig. 4.

In the HNS, compared with $\sigma^*_{rr}, \sigma^*_{\theta\theta}$ and $\sigma^*_{\varphi\varphi}$ play dominant roles to influence the deformation. The surface stress on the outer surface will precompress the nanosphere which can effectively improve the anti-pulverization ability. In contrast, the surface energy of the inner surface will shrink the inner surface. This surface energy aggravates the tensile stress in the inner part of HNS which will induce cracks. However, if the size and shape of electrode are properly chosen, the stress will be well controlled.

In general, the surface energy can contribute to the "size effect" in the stress distribution, so the stress distribution in small size structure is no longer the same as that for the large size. Here, we first investigate the suitable size for the HNS. In the HNS, $\sigma^*_{\theta\theta}$ and $\sigma^*_{\varphi\varphi}$ will be compressive in most outer part of the sphere, while σ^*_{rr} will always be tensile, but play a less important role. Considering silicon will be ductile in nanosize (Gioia & Dai, 2006) and to indicate the total effect of stresses, the effective von Mises stress was introduced through

$$\bar{\sigma}^* = \sqrt{\frac{1}{2}\left[(\sigma^*_{11}-\sigma^*_{22})^2+(\sigma^*_{22}-\sigma^*_{33})^2+(\sigma^*_{33}-\sigma^*_{11})^2\right]} = \sqrt{\frac{1}{2}\left[(\sigma^*_{rr}-\sigma^*_{\theta\theta})^2+(\sigma^*_{\varphi\varphi}-\sigma^*_{rr})^2\right]}, \tag{21}$$

in which $\bar{\sigma}^*$ represents the dimensionless von Mises stress and σ^*_{ii} (ii can be 11, 22 or 33) are the dimensionless principal stresses. The thickness ratio r_i/r_o was fixed to be 0.5, whereas the size of the HNS varies from nanometer to micrometer.

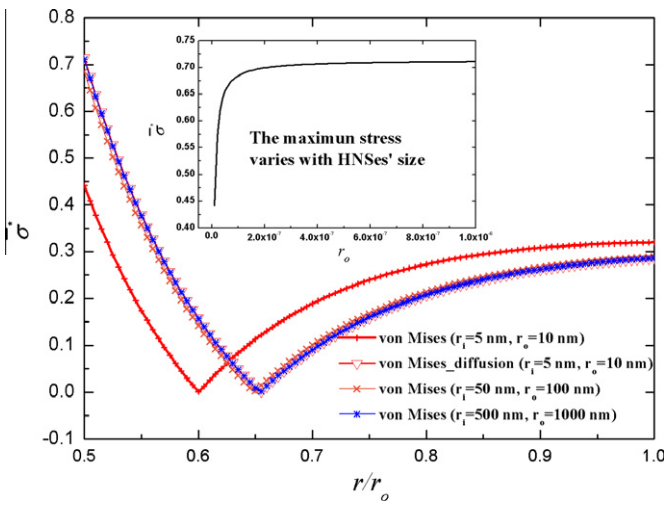

Fig. 5. The von Mises stresses for HNSes with different sizes.

Fig. 5 illustrates the effect of different HNS sizes on the distribution of von Mises stresses. The red crossed line represents the stress in the 10 nm HNS and the hollow triangle line is the stress distribution without considering the surface stress for the same size. Apparently, the surface stress will reduce the magnitude of total stress nearly 58%, that is to say, it can effectively resist pulverization. For different sizes, the stress in the HNSes will increase with respect to the scale of the particle sizes. The insertion indicates the maximum stress variations with respect to the size of HNSes. At nanoscale, the maximum stress is about 67% lower than the microscale particles. It is also evident that the influence of surface effect increases with decreasing particle sizes. Suitable thickness also can minimize the magnitude of the von Mises stress. Fig. 6 shows the several von Mises stress distributions for HNSes with different wall thickness. The blue crossed line represents the stress in the HNS whose inner radius is $r_i = 0.5$ nm and outer radius is $r_o = 10$ nm. The red triangle line and black square one show the stresses with the same outer radius as the blue crossed one, but the inner radii are 0.1 nm and 0.6 nm, respectively. It is obviously that if the wall thickness of HNS is not properly chosen, the HNS will suffer a larger stress.

3.2. Curvature effect on HNS stress distributions

The above all are studies of stress distribution in HNS under special diffusion condition. We have analyzed the size effect and wall thickness effect on stress distribution and mentioned that, in nanoscale, the surface tension of a curved surface will change a lot compared with its planar value. This effect can be revealed through the Tolman length δ. In foregoing work, the δ we adopted in all analyses is calculated by the MD simulation and is assumed to have a small fluctuation. However, it is also

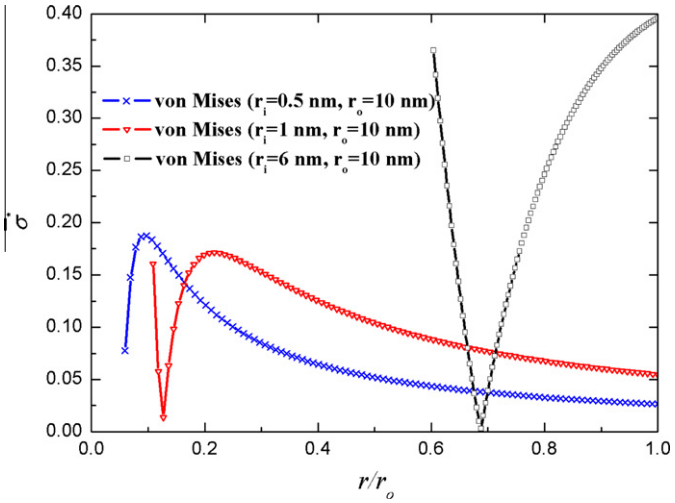

Fig. 6. Stresses distribution for several HNSes with different wall thickness at nanoscale.

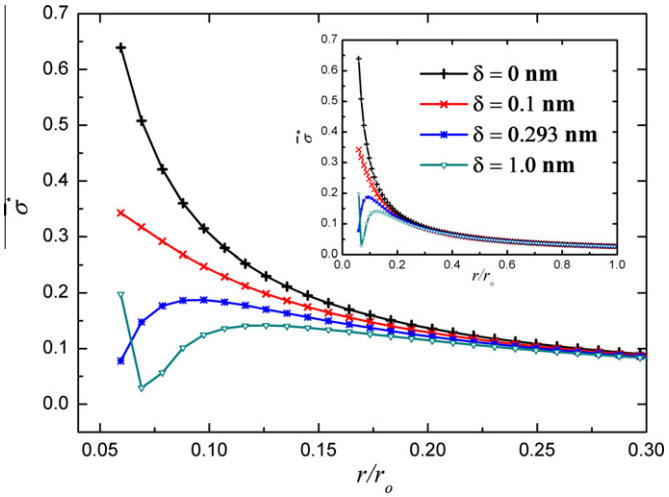

Fig. 7. The stress variation of HNS with respect to the Tolman length.

necessary to know how the Tolman length δ change will affect the stress distribution. For instance, if we change silicon by another material for electrode and using different shape, the Tolman length also will be recalculated. To illustrate the Tolman effect, the δ is assumed to be changed from 0 nm, which means the surface tension will be the planar value, to 1.0 nm.

For comparison, the MD value 0.293 nm for spherical silicon structure is also taken into consideration. A HNS, whose inner radius is r_i = 0.5 nm and outer radius is r_i = 10 nm, is used for indicating the curvature effect. The curvature radius of inner surface is on the same order of δ and the δ/r will be a large quantity in Eq. (10) to influence the surface tension.

Insertion in Fig. 7 shows the von Mises stress distribution along the radial direction with different Tolman length. The stress near the outer surface becomes the same value gradually due to small curvature of outer surface. By contrast, the stresses in the inner part will change a lot. Surface tension decreases with increasing in Tolman length. In other words, if the Tolman length is large enough, the stress induced by surface tension can be diminished and will have small fluctuation along the radial direction. From Fig. 7, we can find that about 30% area near to the inner surface is sensitive with the Tolman length. Most importantly, the peak of stress also appeared in this area. The peak stress will reduce 70% approximately if the Tolman length δ is changed from 0 nm to 1.0 nm.

3.3. NT analysis in stress distributions and curvature effect

Based on what we have analyzed, there are different appropriate size and thickness for HNS under different diffusion condition, which can significantly minimize the stresses, and the curvature changes will also have effect on the stress distribution. Similarly, we have modeled another structure NT, whose inner radius and outer radius are also donated by r_i, r_o. The structure and the symbols are illustrated in Fig. 8.

For comparison and to find a suitable structure for electrode from the mechanical view, the same diffusion condition and material properties of HNS were used in NT analysis. Nevertheless, Tolman length for the tube should be modified. The $\rho(r)$, $p(r)$ in Eqs. (20) are calculated according to the tube. In the simulation, a silicon tube with diameter 5 nm is fully relaxed like what have been done in sphere. Profiles for the density and pressure distribution are plotted in Fig. 9 and the calculated Tolman length is δ = 0.248 nm.

Considering a long enough NT with the symmetrical diffusion process, we can assume that the NT was in the plane-strain state. Using the similar treatments in Eqs. 18,19, the dimensionless Cauchy stresses of NT in cylindrical coordinate system (r,θ,z) (z is the symmetrical axis of NT) can be written as

$$\begin{cases} \sigma^*_{rr} = \left(\frac{\ln\alpha^{-1}}{\ln\alpha_i^{-1}} - \frac{\alpha^{-2}-1}{\alpha_i^{-2}-1}\right) - \frac{\gamma^\infty}{r_o A}\left[\frac{1}{1-\alpha_i^2}\left(\frac{1}{1+2\delta^*}+\frac{\alpha_i^2}{\alpha_i+2\delta^*}\right)\right] + \frac{\gamma^\infty}{r_o A}\frac{\alpha_i^2}{\alpha^2(1-\alpha_i^2)}\left(\frac{1}{1+2\delta^*}+\frac{1}{\alpha_i+2\delta^*}\right) \\ \sigma^*_{\theta\theta} = \left(\frac{\ln\alpha^{-1}-1}{\ln\alpha_i^{-1}} + \frac{\alpha^{-2}+1}{\alpha_i^{-2}-1}\right) - \frac{\gamma^\infty}{r_o A}\left[\frac{1}{1-\alpha_i^2}\left(\frac{1}{1+2\delta^*}+\frac{\alpha_i^2}{\alpha_i+2\delta^*}\right)\right] - \frac{\gamma^\infty}{r_o A}\frac{\alpha_i^2}{\alpha^2(1-\alpha_i^2)}\left(\frac{1}{1+2\delta^*}+\frac{1}{\alpha_i+2\delta^*}\right) \\ \sigma^*_{zz} = \nu\left(\frac{2\ln\alpha^{-1}-1}{\ln\alpha_i^{-1}} + \frac{2}{\alpha_i^{-2}-1}\right) - \left(C_i^*\frac{\ln\alpha^{-1}}{\ln\alpha_i^{-1}} + C_o^*\frac{\ln\alpha_i-\ln\alpha}{\ln\alpha_i}\right) - 2\nu\frac{\gamma^\infty}{r_o A}\frac{1}{1-\alpha_i^2}\left[\left(\frac{1}{1+2\delta^*}+\frac{\alpha_i^2}{\alpha_i+2\delta^*}\right) - \frac{\alpha_i^2}{\alpha^2}\left(\frac{1}{1+2\delta^*}+\frac{1}{\alpha_i+2\delta^*}\right)\right] \end{cases}, \tag{22}$$

and the von Mises stress

$$\bar{\sigma}^* = \sqrt{\frac{1}{2}[(\sigma^*_{11}-\sigma^*_{22})^2 + (\sigma^*_{22}-\sigma^*_{33})^2 + (\sigma^*_{33}-\sigma^*_{11})^2]} = \sqrt{\frac{1}{2}[(\sigma^*_{rr}-\sigma^*_{\theta\theta})^2 + (\sigma^*_{\varphi\varphi}-\sigma^*_{zz})^2 + (\sigma^*_{zz}-\sigma^*_{rr})^2]}. \tag{23}$$

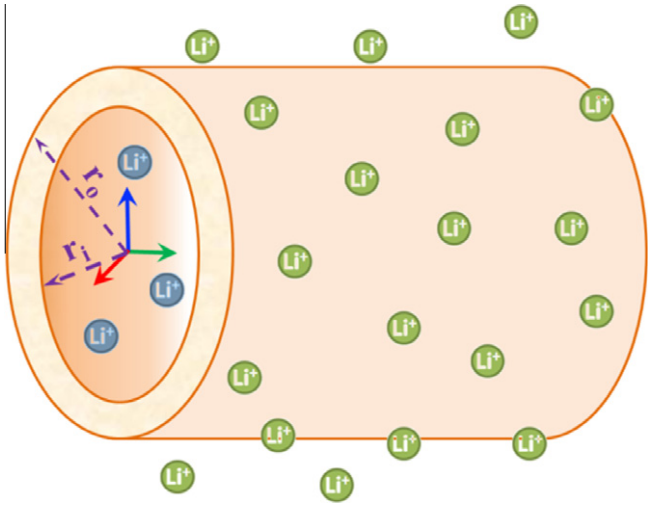

Fig. 8. NT for the nanostructured electrode.

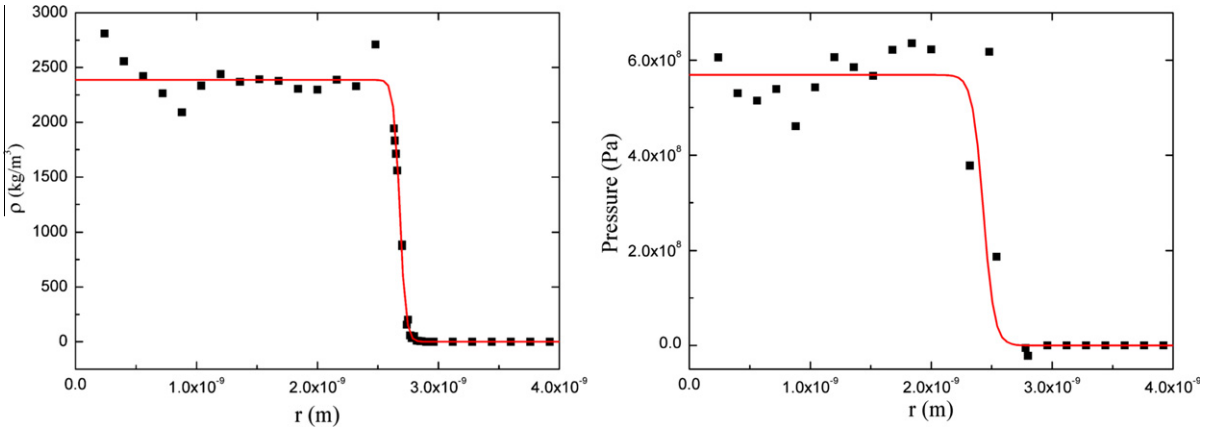

Fig. 9. Density and pressure distributions for the silicon tube along the radius.

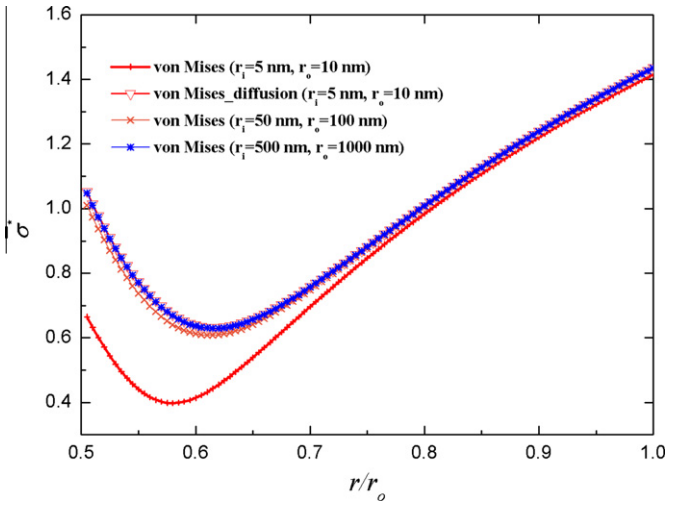

Fig. 10. The von Mises stresses for NTs with different sizes.

Fig. 10 shows the effect of different NT sizes on the von Mises stress distributions. The red crossed line represents the stress in the 10 nm NT and the hollow triangle line is the stress without considering surface stress for the same size. The surface stress will reduce the magnitude of total stress especially in the inner part of the tube. For different sizes, the stress in the NTs will increase with increasing tube sizes. The variation tendency is similar with HNS.

Like what we have analyzed in HNS, we still want to investigate surface tension variation with respect to the curvature change. The inner radius of the tube is r_i = 0.5 nm and outer radius is r_i = 10 nm. The following values of δ will be adopted in our analysis 0 nm, 0.248 nm and 0.5 nm, to get the Tolman effect on the surface energy variation. Fig. 11 is the illustration for von Mises stress distribution near the inner surface whose curvature radius is a quantity on the order of Tolman length. The insertion is the stress distribution for the tube. We can get a similar phenomenon in HNS: the stress will change a lot in the inner area next to the large curvature surface. However, on the outer surface with small curvature, the magnitude of stress will not be affected too much.

3.4. Comparison of HNS and NT in stress distributions and self-buckling

The foregoing work is mainly focused on the sphere and tube separately. The following section, based on what we have obtained, a comparison between two structures was performed. Fig. 12 is the von Mises stress distributions for the HNS and NT whose inner and outer radii are r_i = 5 nm and r_o = 10 nm, respectively. From this graph, we can clearly see that different structures will influence the stress distribution significantly. In the HNS, not only the absolute value of stress is much lower but also the stress fluctuation is much smaller.

In nanostructured electrode design, besides stress analysis, another important issue is self-buckling. Since the surface stress affects the stress distribution in nanostructure obviously, the nanoelectrodes will be self-buckled with the decreasing

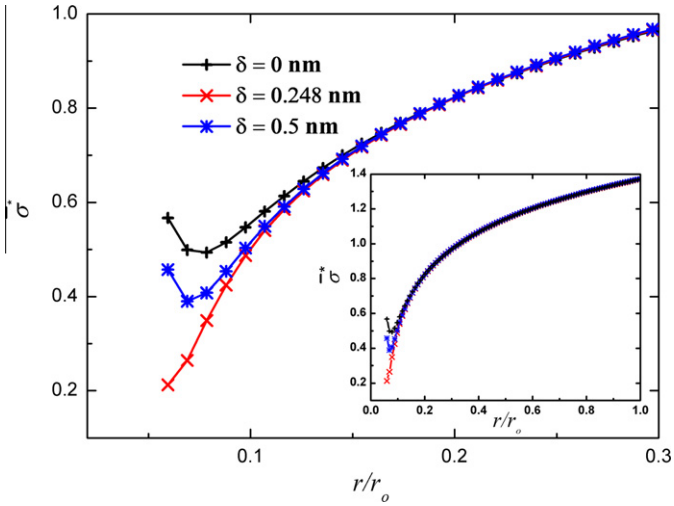

Fig. 11. The stress variation of HNT with respect to the Tolman length.

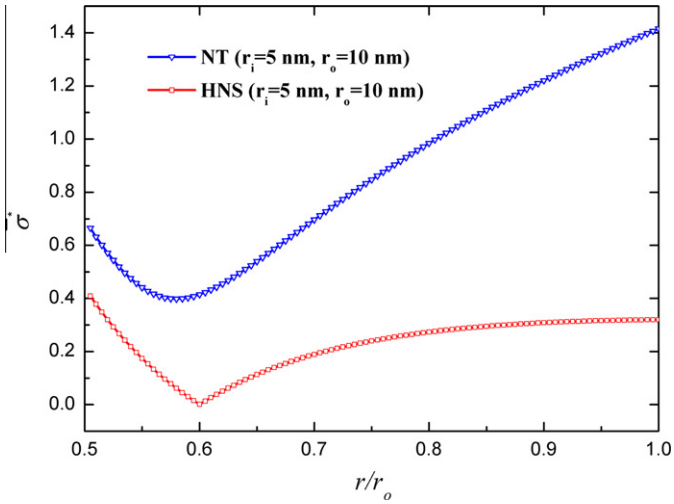

Fig. 12. Comparison of von Mises stresses for HNS and NT.

structure sizes even without insertion and extraction or Li ions. Therefore, the surface stress induced self-buckling should be taken into consideration. Based on the bucking theory in solid structures (Timoshenko & Gere, 1961), we depicted the critical sizes for different wall thicknesses.

For the HNS, using the Tolman length δ to scale all geometric parameters (r is radius of HNS's neutral layer and the h is the wall thickness), the dimensionless critical size with respect to the wall thickness is

$$\frac{r}{h} = \kappa \frac{\frac{h}{\delta} + \sqrt{\left(\frac{h}{\delta}\right)^2 + 16\sqrt{3-3\nu^2}\kappa^{-1}}}{4\sqrt{3-3\nu^2}}, \tag{24}$$

Similarly, we obtain the relationship between the critical sizes and the thicknesses for the NT

$$\left(\frac{r}{h}\right)^3 = \kappa \frac{\left(2+\frac{r}{\delta}\right)}{8(1-\nu^2)}. \tag{25}$$

The meaning of the dimensionless number $\kappa = E\delta/\gamma^{\infty}$ in the last two equations will be given in the following part. Then, we can see the variation of the critical sizes for different thickness of the wall for HNS and NT through Fig. 13.

The thickness varies from 1 nm to 30 nm. The red crossed line represents the critical radius of HNS and the blue triangle line represents the tube's. Then, we can see the variation of the critical sizes for different thickness of the wall for HNS and

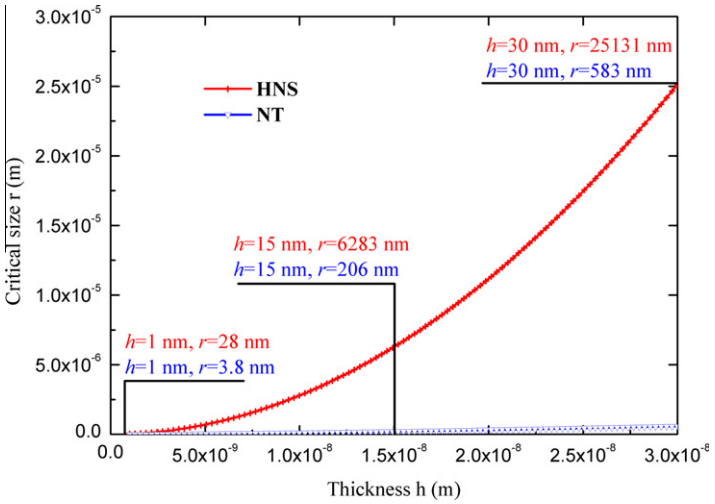

Fig. 13. Critical size for variant thickness for HNS and NT.

NT. When the wall thickness is 1 nm, the radius of HNS should not be larger than 28 nm while for the NT, cannot be larger than 3.5 nm otherwise the nanostructures are self-buckled. When the wall thickness reaches 30 nm, the critical radius for the HNS can be 25.13 μm and for the NT, the critical radius has still in submicron. Therefore, based on the buckling analysis for the same wall thickness, more choices on radius also make the HNS become a suitable structure for electrode.

At last, we emphasize that the quantity γ^{∞}/E in the Eqs. 24,25 is an intrinsic material length. Usually, this length characterized a region near to the surface in which the material mechanical properties will be quite different from the bulk material. In 1963, Mullins (Mullins, 1963) argued that the work, $U(\infty)$, required to separate two adjacent atomic planes of area A can be estimated as the surface-free energy or the elastic work required to move them through a distance y, with the result:

$$\gamma^{\infty}=\frac{U(\infty)}{2A}=\frac{1}{2}\int_0^{R_F}\frac{F_y}{A}dy\approx\frac{E}{2}\int_0^{R_F}\frac{y}{a_0}dy=\frac{E}{4a_0}R_F^2, \tag{26}$$

where a_0 is the lattice spacing, and $R_F\approx 1$ Å is the elastic limit for the separation of the two surfaces. Without loss of generality, we have the rough estimation for the lattice spacing $a_0\approx(2\sim 6)R_F\sim 4R_F$, therefore, we have the order-of-magnitude estimation:

$$\frac{\gamma^{\infty}}{E}=\frac{R_F^2}{4a_0}\sim\frac{a_0}{60}. \tag{27}$$

Mullin's rough estimation above clearly relates the intrinsic material length with the lattice spacing in Eq. (27). Generally speaking, the Tolman length $\delta\approx a_0/2$, then, the dimensionless number we suggested is on the magnitude of

$$\frac{E\delta}{\gamma^{\infty}}\approx 30, \tag{28}$$

That is to say that this dimensionless number is on the order of several tens. In the two typical cases (HNS, NT), the calculated dimensionless number κ is about 23, which is apparently of the same order-of-magnitude as Eq. (28). Considering the meaning of the Tolman length, we can suggest that when a planar surface changed to a curved one, the arrangement of atoms on the surface and next to the surface will reconstruct. As a result, the material properties, the electrons distribution will also have a new state. In the dimensionless number, δ is used to estimate when this "reconstruction effect" should be considered. In the cases (HNS, NT) we analyzed, it is obviously that how this "reconstruction effect" influences the stresses distribution through Figs. 7 and 11.

4. Conclusions

In this paper, we proposed a diffusion and curvature dependent surface elastic model to investigate the diffusion behavior for nanostructured electrodes. In the model, the coupling between the stress and ions diffusion is revealed through the chemical potential variation. The main conclusions of present paper are as follows:

1. To reveal the curvature effect on surface stress, Tolman length δ for the solid structure was introduced. The δ for sphere and tube were calculated through the MD simulation.

2. Using the model, two structures (HNS, NT) were analyzed. On the one hand, we depicted the stress distributions in the two structures for strength analysis; on the other hand, the critical sizes were obtained for different wall thicknesses to make sure the structure is stable. Both analyses promise the HNS will be a more suitable structure for electrode in mechanical view.
3. A new dimensionless number $\kappa = E\delta/\gamma^{\infty}$ is proposed to estimate the relative importance of the Tolman length δ with the intrinsic material length γ^{∞}/E. The dimensionless number is also a dominant parameter in Eqs. (24) and (25) to characterize nanostructure buckling induced by surface tension.

We believed that the nanostructured electrode with suitable structure and size will be self-strengthened by the surface stress which can effectively diminish the silicon anode expansion during insertion and desertion of Li ions. The curvature and diffusion dependent surface model will be an appropriate tool to investigate the diffusion behaviors in nanostructured electrode.

Acknowledgements

This work was jointly supported by the National Natural Science Foundation of China (NSFC, Grant Nos. 60936001, 11072244, 11021262), and the Instrument Developing Project of the Chinese Academy of Sciences (Grant No.Y2010031).

Appendix A. Symbolic descriptions of geometrical and kinematics of a deformable surface

Considering a smooth surface A_0 in the reference configuration in 3D Euclidean space which can be represented by $\mathbf{Y} = \mathbf{Y}(\theta^1, \theta^2)$. $\mathbf{Y}$ is a position vector represent a point on the surface from the origin of the coordinate frame. θ^{α} are curvilinear coordinates on the surface, which α indicate the value 1 or 2. The covariant base vectors $\mathbf{A}_{\alpha}$ of the surface A_0 are defined as

$$\mathbf{A}_{\alpha} = \mathbf{Y}_{,\alpha}. \tag{A1}$$

The comma represents partial derivatives with respect to θ^{α}. The contra-variant base vectors $\mathbf{A}^{\beta}$ of surface A_0 can be defined through

$$\mathbf{A}_{\alpha} \cdot \mathbf{A}^{\beta} = \delta_{\alpha}^{\beta}, \tag{A2}$$

where δ_{α}^{β} is the Kronecker delta in 2D space.

After deformation, the surface A_0 in reference configuration deform to A which is in the current configuration. The vector $\mathbf{Y} = \mathbf{Y}(\theta^1, \theta^2)$ on undeformed surface moved to $\mathbf{y} = \mathbf{y}(\theta^1, \theta^2)$ on deformed surface. Similarly, the covariant base vectors $\mathbf{a}_{\alpha}$ and contra-variant base vectors $\mathbf{a}^{\beta}$ in current configuration can be defined through

$$\mathbf{a}_{\alpha} = \mathbf{y}_{,\alpha}, \tag{A3}$$

$$\mathbf{a}_{\alpha} \cdot \mathbf{a}^{\beta} = \delta_{\alpha}^{\beta}. \tag{A4}$$

A surface deformation gradient tensor $\mathbf{F}_s$ is a linear transformation that maps a vector in the tangent plane of the undeformed surface to a vector in the tangent plane of the deformed surface, which can be defined through

$$\mathbf{F}_s = \mathbf{a}_{\alpha} \otimes \mathbf{A}^{\alpha}. \tag{A5}$$

The Einstein summation convention is adopted in this equation.The inverse transformation of $\mathbf{F}_s$ can be defined as

$$\mathbf{F}_s^{-1} = \mathbf{A}_{\alpha} \otimes \mathbf{a}^{\alpha}. \tag{A6}$$

Therefore, we can deduce some properties of $\mathbf{F}_s$ and $\mathbf{F}_s^{-1}$,

$$\begin{aligned} &\mathbf{F}_s \cdot \mathbf{F}_s^{-1} = \mathbf{I}, \quad \mathbf{F}_s^{-1} \cdot \mathbf{F}_s = \mathbf{I}_0, \\ &\mathbf{F}_s \cdot \mathbf{I}_0 = \mathbf{I} \cdot \mathbf{F}_s = \mathbf{F}_s, \quad \mathbf{F}_s^{-1} \cdot \mathbf{I} = \mathbf{I}_0 \cdot \mathbf{F}_s^{-1} = \mathbf{F}_s^{-1}, \end{aligned} \tag{A7}$$

in which, $\mathbf{I}_0 = \mathbf{A}_{\alpha} \otimes \mathbf{A}^{\alpha}$ and $\mathbf{I} = \mathbf{a}_{\alpha} \otimes \mathbf{a}^{\alpha}$ are identity tensors on the tangent planes of the surface before and after deformations.

The displacement vector $\mathbf{u}$ of a point on the surface either in reference or in current configuration can be written as

$$\mathbf{u} = \mathbf{y} - \mathbf{Y} = u_0^{\alpha}\mathbf{A}_{\alpha} + u_0^{n}\mathbf{N} = u^{\alpha}\mathbf{a}_{\alpha} + u^{n}\mathbf{n}. \tag{A8}$$

The vector $\mathbf{N}$ and $\mathbf{n}$ are unit normal vectors of the surface before and after deformation. u_0^{α} and u_0^{n} (u^{α} and u^{n}) are displacements on tangent plane of surface and normal to the surface, respectively. Notations mentioned above are graphical represented in Fig. A.1.

Furthermore, two surface deformation tensors $\mathbf{C}_s = \mathbf{F}_s^T \cdot \mathbf{F}_s$ and $\mathbf{B}_s^{-1} = \mathbf{F}_s^{-T} \cdot \mathbf{F}_s^{-1}$ can be defined in the reference and the current configurations, and they are both positive-definite. Therefore, the deformation gradient tensor $\mathbf{F}_s$ can be polar decomposed,

$$\mathbf{F}_s = \mathbf{R}_s \cdot \mathbf{U}_s = \mathbf{V}_s \cdot \mathbf{R}_s. \tag{A9}$$

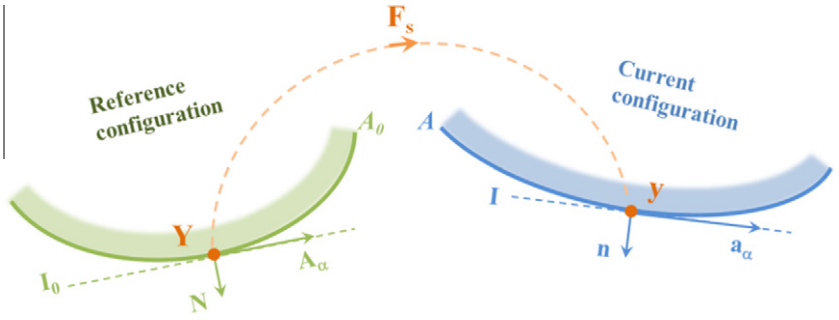

Fig. A.1. Deformation of a surface.

The $\mathbf{U}_s$ and $\mathbf{V}_s$ are defined with $\mathbf{U}_s = \sqrt{\mathbf{C}_s}$ and $\mathbf{V}_s^{-1} = \sqrt{\mathbf{B}_s^{-1}}$, respectively. The $\mathbf{R}_s$ is the two point rotation tensor satisfying

$$\begin{aligned} &\mathbf{R}_S^T \cdot \mathbf{R}_S = \mathbf{I}_0, \quad \mathbf{R}_s \cdot \mathbf{R}_S^T = \mathbf{I}, \\ &\mathbf{R}_S \cdot \mathbf{I}_0 = \mathbf{R}_S, \quad \mathbf{I} \cdot \mathbf{R}_s = \mathbf{R}_s. \end{aligned} \tag{A10}$$

For infinitesimal deformation of surface, the high-order surface displacement gradient will be the small quantities compared to the first-order displacement gradient. Therefore, the high-order small quantities of surface displacement gradient will be neglected and the deformation tensors $\mathbf{C}_s$, $\mathbf{B}_s$ can be expressed as

$$\mathbf{C}_s = \mathbf{I}_0 + 2\mathbf{E}_s, \mathbf{E}_s = \mathbf{I} + 2\boldsymbol{\varepsilon}_s,$$

in which

$$\mathbf{E}_s = \frac{1}{2}(\bar{\nabla}_{0s}\mathbf{u}_0 + \mathbf{u}_0\bar{\nabla}_{0s}), \boldsymbol{\varepsilon}_s = \frac{1}{2}(\bar{\nabla}_s\mathbf{u} + \mathbf{u}\bar{\nabla}_s).$$

The details about operations $\bar{\nabla}_{0s}, \bar{\nabla}_s$ and more geometry and kinematics of the surface can be found in Wang et al. (2010), Wang and Zhao (2011).

References

Altenbach, H., & Eremeyev, V. A. (2011). On the shell theory on the nanoscale with surface stresses. *International Journal Engineering Sciences, 49*, 1294–1301.

Altenbach, H., Eremeyev, V. A., & Morozov, N. F. (2009). Linear theory of shells taking into account surface stresses. *Doklady Physics, 54*, 531–535.

Altenbach, H., Eremeyev, V. A., & Morozov, N. F. (2010). On equations of the linear theory of shells with surface stresses taken into account. *Mechanics of Solids, 45*, 331–342.

Belova, I. V., & Murch, G. E. (1995). Thermal and diffusion-induced stresses in crystalline solids. *Journal of Applied Physics, 77*, 127–134.

Boukamp, B. A., Lesh, G. C., & Huggins, R. A. (1981). All-solid lithium electrodes with mixed-conductor matrix. *Journal of Electrochemical Society, 128*, 725–729.

Bruce, P. G., Scrosati, B., & Tarascon, J. M. (2008). Nanomaterials for rechargeable lithium batteries. *Angewandte Chemie-International Edition, 47*, 2930–2946.

Chan, C. K., Peng, H. L., Liu, G., McIlwrath, K., Zhang, X. F., Huggins, R. A., & Cui, Y. (2008). High-performance lithium battery anodes using silicon nanowires. *Nature Nanotechnology, 3*, 31–35.

Cheng, Y. T., & Verbrugge, M. W. (2008). The influence of surface mechanics on diffusion induced stresses within spherical nanoparticles. *Journal of Applied Physics, 104*, 083521.

Cheng, Y. T., & Verbrugge, M. W. (2009). Evolution of stress within a spherical insertion electrode particle under potentiostatic and galvanostatic operation. *Journal of Power Sources, 190*, 453–460.

Chu, J. L., & Lee, S. B. (1994). The effect of chemical stresses on diffusion. *Journal of Applied Physics, 75*, 2823–2829.

Gibbs, J. W. (1961). On the equilibrium of heterogeneous substances. In J. W. Gibbs (Ed.), *The Scientific Papers of Thermodynamics* (pp. 55–353). New York: Dover.

Gioia, G., & Dai, X. (2006). Surface stress and reversing size effect in the initial yielding of ultrathin films. *Journal of Applied Mechanics-Transactions of the ASME, 73*, 254–258.

Gurtin, M. E., & Murdoch, A. I. (1978). Surface stress in solids. *International Journal of Solids and Structure, 14*, 431–440.

Haftbaradaran, H., Gao, H. J., & Curtin, W. A. (2010). A surface locking instability for atomic intercalation into a solid electrode. *Applied Physics Letters, 96*, 091909.

Hara, S., Izumi, S., Kumagai, T., & Sakai, S. (2005). Surface energy, stress and structure of well-relaxed amorphous silicon: A combination approach of *ab initio* and classical molecular dynamics. *Surface Science, 585*, 17–24.

He, X. M., Pu, W. H., Wang, L., Ren, J. G., Jiang, C. Y., & Wan, C. R. (2007). Synthesis of nano Sb-encapsulated pyrolytic polyacrylonitrile composite for anode material in lithium secondary batteries. *Electrochimica Acta, 52*, 3651–3653.

Hoger, A. (1986). On the determination of residual-stress in an elastic body. *Journal of Elasticity, 16*, 303–324.

Hu, Y., Zhao, X., & Suo, Z. (2010). Averting cracks caused by insertion reaction in lithium-ion batteries. *Journal of Materials Research, 25*, 1007–1010.

Kasavajjula, U., Wang, C. S., & Appleby, A. J. (2007). Nano- and bulk-silicon-based insertion anodes for lithium-ion secondary cells. *Journal of Power Sources, 163*, 1003–1039.

Kwon, Y., Kim, M. G., Kim, Y., Lee, Y., & Cho, J. P. (2006). Effect of capping agents in tin nanoparticles on electrochemical cycling. *Electrochemical and Solid State Letters, 9*, A34–A38.

Li, J., Dozier, A. K., Li, Y., Yang, F. Q., & Cheng, Y.-T. (2011). Crack pattern formation in thin film lithium-ion battery electrodes. *Journal of Electrochemical Society, 158*, A689–A694.

Li, J. C. M., & Mehl, R. F. (1978). Physical-chemistry of some microstructural phenomena. *Metallurgical and Material Transactions A-Physical Metallurgy and Materials Science, 9*, 1353–1380.

Mandell, M. J., & Reiss, H. (1975). Thermodynamics of curved boundary layers. *Journal of Statistical Physics, 13*, 107–112.

Miller, R. E., & Shenoy, V. B. (2000). Size-dependent elastic properties of nanosized structural elements. *Nanotechnology, 11*, 139–147.
Mullins, W. W. (1963). Solid surface morphologies governed by capillarity. In W. M. Robertson & N. A. Gjostein (Eds.), *Metal surfaces: Structure, energetics and kinetics* (pp. 17–66). Ohio: ASM Metals Park.
Nazri, G. A., & Pistoia, G. (2003). *Lithium batteries: Science and technology*. New York: Springer.
Nose, S. (1984). A unified formulation of the constant temperature molecular-dynamics methods. *Journal of Chemical Physics, 81*, 511–519.
Paukshto, M. V. (1999). Diffusion-induced stresses in solids. *International Journal of Fracture, 97*, 227–236.
Plimpton, S. (1995). Fast parallel algorithms for short-range molecular-dynamics. *Journal of Computational Physics, 117*, 1–19.
Shenoy, V. B., Johari, P., & Qi, Y. (2010). Elastic softening of amorphous and crystalline Li–Si phases with increasing Li concentration: A first-principles study. *Journal of Power Sources, 195*, 6825–6830.
Song, T., Xia, J. L., Lee, J. H., Lee, D. H., Kwon, M. S., Choi, J. M., Wu, J., Doo, S. K., Chang, H., Il Park, W., Zang, D. S., Kim, H., Huang, Y. G., Hwang, K. C., Rogers, J. A., & Paik, U. (2010). Arrays of sealed silicon nanotubes as anodes for lithium ion batteries. *Nano Letters, 10*, 1710–1716.
Teki, R., Datta, M. K., Krishnan, R., Parker, T. C., Lu, T. M., Kumta, P. N., & Koratkar, N. (2009). Nanostructured silicon anodes for lithium ion rechargeable batteries. *Small (Weinheim an der Bergstrasse, Germany), 5*, 2236–2242.
Tersoff, J. (1988). New empirical approach for the structure and energy of covalent systems. *Physical Review B, 37*, 6991–7000.
Thompson, S. M., Gubbins, K. E., Walton, J., Chantry, R. A. R., & Rowlinson, J. S. (1984). A molecular-dynamics study of liquid-drops. *Journal of Chemical Physics, 81*, 530–542.
Timoshenko, S. P., & Gere, J. M. (1961). *Theory of elastic stability* (2nd ed.). New York: McGraw-Hill.
Tolman, R. C. (1949). The effect of droplet size on surface tension. *Journal of Chemical Physics, 17*, 333–337.
Wang, Z. Q., & Zhao, Y. P. (2011). Thermo-hyperelastic models for nanostructured materials. *Science China-Physics Mechanics and Astronomy, 54*, 948–956.
Wang, Z. Q., Zhao, Y. P., & Huang, Z. P. (2010). The effects of surface tension on the elastic properties of nano structures. *International Journal Engineering Sciences, 48*, 140–150.
Yang, F. Q. (2012). Diffusion-induced stress in inhomogeneous materials: concentration-dependent elastic modulus. *Science China-Physics Mechanics and Astronomy, 55*, 955–962.
Yang, F. Q. (2010). Insertion-induced breakage of materials. *Journal of Applied Physics, 108*, 073536.